

Quark distributions in the nucleon based on a relativistic 3-body approach to the NJL model

H. Mineo, W. Bentz, K. Yazaki

Department of Physics,

Faculty of Science

University of Tokyo

Hongo 7-3-1, Bunkyo-ku, Tokyo 113, Japan

Abstract

Quark light cone momentum distributions in the nucleon are calculated in a relativistic 3-body approach to the NJL model by using a simple 'static approximation' for the Faddeev kernel. A method is presented which automatically satisfies the number and momentum sum rules, even in the regularized theory. In order to assess the sensitivity to the regularization scheme, two schemes which can be formulated in terms of light cone variables are discussed. The effects of the (composite) pion cloud are taken into account in a convolution approach, and the violation of the Gottfried sum rule is discussed. After performing the Q^2 evolution, the resulting distributions are compared to the empirical ones.

PACS numbers: 12.39-x, 12.39.Ki, 14.20.Dh

Keywords: Structure functions, Effective quark theories

¹Correspondence to: W. Bentz, E-mail: bentz@phys.s.u-tokyo. ac.jp

1 Introduction

Deep inelastic lepton-nucleon scattering experiments are providing detailed information on the quark and gluon distributions in the nucleon [1]. By analyzing the distribution functions derived from the measured cross sections with the help of the Q^2 evolution based on perturbative QCD, one can extract the fraction of the nucleon's momentum and spin carried by the quarks at some renormalization scale μ , and obtain valuable information on the spin-flavor structure of the nucleon [2]. For example, of great interest in this connection are the flavor dependences of the valence quark distributions [3] and of the sea quark distributions [4, 5], which reflect the roles of qq (diquark) and $\bar{q}q$ (mesonic) correlations in the nucleon. Current experiments at HERA are exploring the region of small x in order to get more information on large-distance (non-perturbative) phenomena, and future experiments at RHIC will concentrate on the spin distributions.

An essential tool to analyze the data on the nucleon structure functions in the Bjorken limit are the factorization theorems [6], which allow us to separate the long-distance parts (parton distributions) from the short-distance parts (hard scattering cross sections). The latter ones are calculable from perturbative QCD, while the parton distributions require the knowledge of the nucleon wave function. The central point of the factorization theorems is that the infrared-divergent (long-distance) contributions to the perturbative diagrams can be absorbed into the definition of 'renormalized' parton distributions [2]. Due to this procedure, the parton distributions eventually depend on a factorization scale (μ), which is usually taken to be the same as the renormalization scale. The requirement that the structure functions

should not depend on this scale then leads to the famous DGLAP equations [7] for the μ dependence of the distribution functions, which in turn also determines the Q^2 dependence of the structure functions. One can therefore use effective quark theories to calculate the distribution functions at some 'low energy scale' $\mu = Q_0$, where a description in terms of quark degrees of freedom alone is expected to be valid, and then use the DGLAP equations to relate them to the distribution functions extracted from experimental data at $\mu = Q$.

As an effective quark theory in the low energy region, the Nambu - Jona-Lasinio (NJL) model [8] is a powerful tool to investigate the properties of hadrons [9]. It exhibits the spontaneous breaking of chiral symmetry in a simple and clear way, and allows the solution of the relativistic two- and three-body equations in the ladder approximation due to the simplicity of the interaction [10, 11]. Concerning the ground state properties of baryons, the Faddeev approach to the NJL model has been quite successful [12], and since in this approach the translational invariance and covariance are preserved, it is natural to apply it also to the structure functions of the nucleon.² Actually, the NJL model has been formulated recently on the light cone (LC) and the structure function of the pion has been calculated [15]. For the case of the nucleon, however, there is the problem that the relativistic Faddeev equations are usually solved by performing a Wick rotation using the Euclidean sharp cut-off [10], and this method cannot be applied directly to the calculation of the LC momentum distributions. A possibility is first to go to the moment space and then re-construct the distribution functions

²There are already several investigations of the nucleon structure functions using the soliton approach to the NJL model [13]. For a calculation using the Bethe-Salpeter equation for a quark and a structureless diquark, see ref. [14].

by the inverse Mellin transformation. While such a calculation is now in progress [16], it is desirable for a first orientation to use some simple approximation which allows a direct calculation of the distributions. The 'static approximation' to the Faddeev kernel [17, 18], which amounts to neglect the momentum dependence of the propagator of the exchanged quark, allows an analytic solution of the Faddeev equation, and it has been shown in ref. [18] that for the nucleon mass this approximation is not unreasonable. However, the overbinding of the nucleon compared to the exact Faddeev result and the 'point-like' quark-diquark interaction lead to radii which are too small [19], and therefore we can expect that the resulting momentum distributions will be too stiff. However, our main purpose here is to see some general trends, to investigate the influence of the regularization scheme and to demonstrate that in the Faddeev approach the validity of the number and momentum sum rules is guaranteed from the outset, which is not the case in the soliton or bag model approaches. The calculation employing the static approximation to the Faddeev kernel resembles the quark-diquark calculations performed earlier [20]. We will go beyond these calculations by including the structure of the diquark (and also of the pion when estimating the pionic cloud effects), and investigating the sensitivity to the regularization scheme while preserving the number and momentum sum rules.

The rest of this paper is organized as follows: In sect. 2 we explain the model for the nucleon wave function, in sect. 3 we explain our method to calculate the quark distribution functions, and in sect. 4 we discuss the numerical results. A summary is presented in sect. 5.

2 NJL model for the nucleon wave function

The NJL model is characterized by a chirally symmetric four-Fermi interaction lagrangian \mathcal{L}_I . By means of Fierz transformations, one can rewrite any \mathcal{L}_I into a form where the interaction strength in a particular $\bar{q}q$ or qq channel can be read off directly [10]. That part which generates the constituent quark mass M_Q and the pion as a collective $\bar{q}q$ bound state is given by

$$\mathcal{L}_{I,\pi} = \frac{1}{2}g_\pi \left((\bar{\psi}\psi)^2 - (\bar{\psi}(\gamma_5\boldsymbol{\tau})\psi)^2 \right), \quad (2.1)$$

and that which describes the qq interaction in the scalar diquark ($J^\pi = 0^+, T = 0$) channel is

$$\mathcal{L}_{I,s} = g_s \left(\bar{\psi}(\gamma_5 C) \tau_2 \beta^A \bar{\psi}^T \right) \left(\psi^T (C^{-1} \gamma_5) \tau_2 \beta^A \psi \right), \quad (2.2)$$

where $\beta^A = \sqrt{3/2} \lambda^A$ ($A = 2, 5, 7$) are the color $\bar{3}$ matrices, and $C = i\gamma_2\gamma_0$. The coupling constants g_π and g_s are related to the ones appearing in the original \mathcal{L}_I by numerical factors due to the Fierz transformation, but instead of choosing a particular form of \mathcal{L}_I we will treat g_π and the ratio $r_s = g_s/g_\pi$ as free parameters, where the latter reflects different possible forms of \mathcal{L}_I [10].

The reduced t-matrices in the pionic and scalar diquark channels are obtained from the respective Bethe-Salpeter (BS) equations as [10]

$$\tau_\pi(k) = \frac{-2ig_\pi}{1 + 2g_\pi\Pi_\pi(k)}, \quad \tau_s(k) = \frac{4ig_s}{1 + 2g_s\Pi_s(k)} \quad (2.3)$$

with the bubble graph

$$\Pi_\pi(k) = \Pi_s(k) = 6i \int \frac{d^4q}{(2\pi)^4} tr_D \left[\gamma_5 S(q) \gamma_5 S(q-k) \right], \quad (2.4)$$

where $S(q) = \frac{1}{\not{q} - M_Q + i\epsilon}$ is the Feynman propagator and M_Q the constituent quark mass.

If the interacting two-body channels are restricted to the scalar diquark one, the relativistic Faddeev equation [10] can be reduced to an effective BS equation for a composite scalar diquark and a quark, interacting via quark exchange [21]. As we explained in the previous section, in this paper we will restrict ourselves to the static approximation [17, 18], where the Feynman propagator in the quark exchange kernel is simply replaced by $-1/M_Q$. Then the effective BS equation reduces to a geometric series of quark-diquark bubble graphs ($\Pi_N(p)$), and the solution for the t-matrix in the color singlet channel is

$$T(p) = \frac{3}{M_Q} \frac{1}{1 + \frac{3}{M_Q} \Pi_N(p)} \quad (2.5)$$

with

$$\Pi_N(p) = - \int \frac{d^4k}{(2\pi)^4} S(k) \tau_s(p-k). \quad (2.6)$$

The quark-diquark vertex function $\Gamma_N(p)$ in the covariant normalization is then obtained from the pole behaviour $T \rightarrow \sum_s \Gamma_N(p_s) \bar{\Gamma}_N(p_s) / (p^2 - M_N^2 + i\epsilon)$, where M_N is the nucleon mass, as ³

$$\Gamma_N(p) = Z_N u_N(p) \quad (2.7)$$

$$Z_N = \left(\frac{1}{\partial \Pi_N(p) / \partial \not{p} \Big|_{p=M_N}} \right)^{\frac{1}{2}} = \left(\frac{p_- / M_N}{\bar{u}_N(p) \frac{\partial \Pi_N(p)}{\partial p_+} u_N(p)} \right)^{\frac{1}{2}}, \quad (2.8)$$

where $u_N(p)$ is a free Dirac spinor with mass M_N normalized by $\bar{u}_N(p) u_N(p) =$

³Our conventions for LC variables are $a^\pm = \frac{1}{\sqrt{2}} (a^0 \pm a^3)$, $a_\pm = \frac{1}{\sqrt{2}} (a_0 \pm a_3)$, and $a_\perp^i = -a_{\perp i}$ ($i = 1, 2$). The Lorentz scalar product is $a \cdot b = a_+ b^+ + a_- b^- - \mathbf{a}_\perp \cdot \mathbf{b}_\perp$. We will frequently call $p_-(p_+)$ the 'LC minus (plus) component' of the four vector p .

$2M_N$. In this normalization, the vertex function satisfies the relation

$$\frac{1}{2p_-} \bar{\Gamma}_N(p) \frac{\partial \Pi_N(p)}{\partial p_+} \Gamma_N(p) = 1, \quad (2.9)$$

which leads to charge and baryon number conservation in any treatment which preserves the Ward identity

$$\Lambda_{q/P}^+(p, p) = \frac{\partial \Pi_N(p)}{\partial p_+} N_{q/P} \quad (2.10)$$

for the vertex of the quark number current of the proton at $q = 0$ ($N_{u/P} = 2$, $N_{d/P} = 1$).⁴

3 Quark distribution functions

The twist-2 quark LC momentum distribution in the proton (momentum p) is defined as [22, 23]

$$\tilde{f}_{q/P}(x) = \frac{1}{2} \int \frac{dz^-}{2\pi} e^{ip-xz^-} \langle p | T (\bar{\psi}_q(0) \gamma^+ \psi_q(z^-)) | p \rangle, \quad (3.1)$$

where q denotes the quark flavor, $|p\rangle$ is the proton state, and x is the Bjorken variable which corresponds to the fraction of the proton's LC momentum component p_- carried by the quark q . As has been discussed in detail in ref. [22, 23], for connected LC correlation functions the T-product is identical to the usual product, from which it follows that the distribution (3.1) is non-zero in the interval $-1 < x < 1$. The physical quark and antiquark distributions which determine the structure functions F_1 and F_2 are obtained for $0 < x < 1$ as $f_{q/P}(x) = \tilde{f}_{q/P}(x)$ and $f_{\bar{q}/P}(x) = -\tilde{f}_{q/P}(-x)$. The valence (v) and sea (s) quark distributions are then given by $f_{qv/P}(x) = f_{q/P}(x) - f_{\bar{q}/P}(x)$, $f_{qs/P}(x) = f_{\bar{q}/P}(x) = f_{\bar{q}/P}(x)$.

⁴This vertex is defined by $\langle p | \bar{\psi}(0) \gamma^+ \frac{1 \pm \tau_z}{2} \psi(0) | p \rangle = \bar{\Gamma}_N(p) \Lambda_{q/P}^+(p, p) \Gamma_N(p)$ for $q = u(d)$.

The evaluation of the distribution (3.1) can be reduced to a straight forward Feynman diagram calculation by noting that it can be expressed as [22, 23, 24]⁵

$$\tilde{f}_{q/P}(x) = -\frac{i}{2p_-} \int \frac{d^4k}{(2\pi)^4} \delta(x - \frac{k_-}{p_-}) Tr_D \gamma^+ M_q(p, k), \quad (3.2)$$

with the quark 2-point function in the proton given by

$$M_{q,\beta\alpha}(p, k) = i \int d^4z e^{ikz} \langle p|T(\bar{\psi}_{q,\alpha}(0)\psi_{q,\beta}(z))|p\rangle. \quad (3.3)$$

We therefore have to evaluate the Feynman diagrams for the quark propagator in the nucleon, trace it with γ^+ , fix the LC minus component of the quark momentum as $k_- = p_-x$ and integrate over the remaining components k_+ and \mathbf{k}_\perp . Since in our model for the nucleon discussed in the previous section the quark can either appear as a spectator or as a constituent of the scalar diquark, the Feynman diagrams to be evaluated are shown in fig.1. (In the full Faddeev approach, there is also a diagram where the external operator acts on the exchanged quark, but in the present static approximation this diagram does not contribute.)

To present the formulae for the diagrams fig.1, we note that the second diagram (the diquark contribution) can be expressed conveniently as a convolution integral if we insert the identity

$$1 = \int dy \int dz \int dq_0^2 \delta(y - \frac{q_-}{p_-}) \delta(z - \frac{k_-}{q_-}) \delta(q^2 - q_0^2), \quad (3.4)$$

i.e; y is the fraction of the nucleon's momentum component p_- carried by the diquark, z is the fraction of the diquark's momentum component q_- carried

⁵The original Lorentz invariant expression is recovered by $k_-/p_- \rightarrow k \cdot q/p \cdot q$ and $\gamma^+/p_- \rightarrow \not{q}/p \cdot q$. The expression (3.2) corresponds to the Bjorken limit in the frame where $\mathbf{q}_\perp = 0$, $q_z < 0$, i.e; $q_+ \rightarrow \infty$, $q_- \rightarrow -p_-x$.

by the quark inside the diquark ($x = yz$), and q_0^2 is the virtuality of the diquark. Using also the identity

$$S(k)\gamma^+S(k) = -\frac{\partial S(k)}{\partial k_+}, \quad (3.5)$$

and performing partial integrations in the plus components of the loop momenta, which is permissible since these integrations are convergent and not restricted by the regularization schemes to be discussed later, we obtain the following expression⁶:

$$f_{Q/P}(x) = \delta_{Q,U} F_{Q/P}(x) + \frac{1}{2}F_{Q(D)/P}(x). \quad (3.6)$$

Here the first term corresponds to the first diagram in fig.1 and is expressed as

$$F_{Q/P}(x) = \frac{1}{2p_-} \bar{\Gamma}_N \left(\frac{\partial}{\partial p_+} \Pi_N(x, p) \right) \Gamma_N, \quad (3.7)$$

where $\Pi_N(x, p)$ is the quark-diquark bubble graph for fixed minus component of the quark momentum:

$$\Pi_N(x, p) = - \int \frac{d^4k}{(2\pi)^4} \delta(x - \frac{k_-}{p_-}) S(k) \tau_s(p - k). \quad (3.8)$$

The second term in (3.6) corresponding to the second diagram in fig.1 is purely isoscalar and given by the convolution integral

$$F_{Q(D)/P}(x) = \int_0^1 dy \int_0^1 dz \delta(x - yz) \int_{-\infty}^{\infty} dq_0^2 F_{Q/D}(z, q_0^2) F_{D/P}(y, q_0^2), \quad (3.9)$$

where the distributions $F_{Q/D}(z, q_0^2)$ and $F_{D/P}(y, q_0^2)$ for fixed virtuality of the diquark (D) are expressed as

$$F_{Q/D}(z, q_0^2) = -2g^2(q_0^2) \frac{\partial \Pi_s(z, q_0^2)}{\partial q_0^2} \quad (3.10)$$

⁶To distinguish the case without the pion cloud (valence quark picture) from that including the pion cloud, we replace $q \rightarrow Q$ in the formulae corresponding to the diagrams of fig.1.

$$F_{D/P}(y, q_0^2) = \bar{\Gamma}_N \left(\frac{1}{2p_-} \frac{\partial}{\partial p_+} + y \frac{\partial}{\partial q_0^2} \right) \Pi_N(y, q_0^2; p) \Gamma_N. \quad (3.11)$$

Here $\Pi_s(z, q_0^2)$ is the quark-quark bubble graph for fixed minus momentum component of the quark, $g^2(q_0^2) = -1 / \left(\frac{\partial \Pi_s(q_0^2)}{\partial q_0^2} \right)$ is the quark-diquark coupling constant, and $\Pi_N(y, q_0^2; p)$ is the quark-diquark bubble graph for fixed virtuality and minus momentum component of the diquark:

$$\Pi_s(z, q_0^2) = \left[6i \int \frac{d^4 k}{(2\pi)^4} \delta(z - \frac{k_-}{q_-}) \text{tr}_D (\gamma_5 S(k) \gamma_5 S(k - q)) \right]_{q^2=q_0^2} \quad (3.12)$$

$$\Pi_N(y, q_0^2; p) = - \int \frac{d^4 q}{(2\pi)^4} \delta(y - \frac{q_-}{p_-}) \delta(q^2 - q_0^2) S(p - q) \tau_s(q). \quad (3.13)$$

If we use the dispersion representation for the diquark t-matrix τ_s , we can perform the k_+ and q_+ integrals analytically and verify that the distribution (3.6) is non-zero only in the interval $0 < x < 1$. This fact was anticipated already in our notation ($\tilde{f}_{Q/P}(x) = f_{Q/P}(x)$) and in the integration limits in eq. (3.9), and corresponds to a valence quark model ($f_{\bar{Q}/P}(x) = 0$).

Using the above expressions and the normalization (2.9), it is a simple matter to confirm the validity of the number and momentum sum rules ⁷

$$\int_0^1 dx f_{Q/P}(x) = N_{Q/P} \quad (3.14)$$

$$\int_0^1 dx \cdot x (f_{U/P}(x) + f_{D/P}(x)) = 1. \quad (3.15)$$

In more general terms, what we have really confirmed here is the validity of the Ward identities for quark number and momentum conservation: Concerning the number conservation, if we integrate the distribution function of

⁷To verify these relations, it is only necessary to note that the relations $\int_0^1 dz F_{Q/D}(z, q_0^2) = 2$ and $\int_0^1 dz \cdot z F_{Q/D}(z, q_0^2) = 1$ hold for any q_0^2 (here $F_{Q/D}(z, q_0^2)$ is symmetric around $z = 1/2$), and therefore the second term in eq. (3.11) gives a vanishing surface term when integrated over q_0^2 . The sum rules are then obvious since the integral of $\Pi_N(y, q_0^2, p)$ over q_0^2 reduces to $\Pi_N(1 - y, p)$, and that of $\Pi_N(x, p)$ over x to $\Pi_N(p)$.

fig.1 over x , the restriction $k_- = p_-x$ is lifted, and the diagrams correspond to $\Lambda_{Q/P}^+(p, p)/2p_-$. The validity of the Ward identity (2.10) follows then from (3.5) and partial integrations in the plus components of the loop momenta. A similar argument holds for the Ward identity expressing momentum conservation. Therefore, the Ward identities and the sum rules (3.14), (3.15) hold in any regularization scheme which does not restrict the LC plus components of the loop momenta. The regularization schemes to be discussed at the end of this section satisfy this requirement.

As we have noted above, the model described so far gives essentially only valence-like distributions at the low energy scale. Although sea quark distributions will be generated in the process of the Q^2 evolution, those will be flavor independent ($f_{\bar{u}/P} = f_{\bar{d}/P}$), which contradicts the experimentally measured violation of the Gottfried sum rule [1]. Also, it is a general trend of valence quark models that the resulting valence quark distributions are too stiff (too strongly pronounced peak and too small support at low values of x). We therefore consider here the effects of the pion dressing of the constituent quarks, as has been done also in previous works [25]. (For a recent investigation using the LC quantization, see ref. [26].) In order to take into account the pion cloud, in principle we should solve the Schwinger-Dyson equation for the quark Feynman propagator $S(q) = \frac{1}{\not{q} - M_Q - \Sigma_Q(p)}$, where

$$\Sigma_Q(p) = -3 \int \frac{d^4k}{(2\pi)^4} (\gamma_5 S(k) \gamma_5) \tilde{\tau}_\pi(p - k) \equiv -\Pi_Q(p) \quad (3.16)$$

is the quark self energy due to the pion cloud, and the reduced pion t-matrix $\tilde{\tau}_\pi \equiv \tau_\pi + 2ig_\pi$ depends also on $S(p)$. This propagator should then be used to calculate the diquark t-matrix τ_s and the nucleon vertex function Γ_N . Using these modified propagators and vertex functions, one should, in addition to

the diagrams of fig.1, also evaluate the diagrams of fig.2, where the operator insertion is made on the quark while the pion is 'in flight', or on the quark and the antiquark in the pion.

Clearly, such a calculation is very complicated, and the usually employed convolution formalism [25] involves the following two major approximations: First, pionic effects can be renormalized into a re-definition of the constituent quark mass and the four fermi coupling constants if one approximates the quark propagator by its pole part ⁸

$$S(p) = \frac{Z_Q}{\not{p} - \hat{M}_Q + i\epsilon} \equiv Z_Q \hat{S}(p) \quad (3.17)$$

with

$$Z_Q = \left(1 + \frac{\partial \Pi_Q}{\partial \not{k}} \Big|_{k=\hat{M}_Q} \right)^{-1}. \quad (3.18)$$

If we define 'renormalized' coupling constants \hat{G}_α by $G_\alpha = \hat{G}_\alpha/Z_Q^2$ ($\alpha = \pi, s$), it is easy to see that the Green functions and vertex functions are renormalized according to $\tau_\alpha = \hat{\tau}_\alpha/Z_Q^2$, $T = Z_Q \hat{T}$, $\Gamma_N = \sqrt{Z_Q} \hat{\Gamma}_N$. If we then impose the same conditions on the parameters as commonly used in the case without pion cloud effects (that is, $f_\pi = 93MeV$, $m_\pi = 140MeV$, $\hat{M}_Q = 300 - 500MeV$, and $M_N = 940MeV$), the cut-off and the coupling constants \hat{G}_α take the same values as in the case without pionic cloud effects. (In terms of the lagrangian, such a renormalization procedure corresponds to writing $G(\bar{\psi}\psi)^2 = \hat{G}(\bar{\hat{\psi}}\hat{\psi})^2$ with $\psi = \sqrt{Z_Q} \hat{\psi}$ and $G = \hat{G}/Z_Q^2$.) It is also easy to check that all diagrams in fig.1 and fig.2 get a factor Z_Q .

⁸Green functions and vertex functions which differ from those without pionic effects by the replacements $M_Q \rightarrow \hat{M}_Q$, $G_\alpha \rightarrow \hat{G}_\alpha \equiv G_\alpha Z_Q^2$ ($\alpha = \pi, s$) will be denoted by a hat. Since due to the discussion following eq.(3.18) these renormalized quantities are numerically equivalent to the ones used previously, this distinction will eventually be dropped.

If one then calculates the diagrams of fig.2 in terms of these renormalized quantities and writes the results in terms of a convolution integral, one finds that due to the Dirac structure of the insertions on the 'parent' quark line there appear three convolutions terms [27]. Only one of them involves the generalization of the 'bare' quark distribution in the nucleon (eq.(3.6)) to the off shell case ($f_{Q/P}(x) \rightarrow f_{Q/P}(x, k_0^2)$, where k_0^2 is the virtuality of the parent quark), convoluted with the quark distribution within the parent quark. Each of the other two terms involve one additional factor of $(k_0^2 - M_Q^2)$ in the integrand compared to the first term, which has a sharp peak at $k_0^2 = M_Q^2$. The second approximation commonly used is therefore to neglect these two terms, and to assume that due to the sharp peak of $f_{Q/P}(x, k_0^2)$ the quark distribution within the parent quark can be evaluated at $k_0^2 = M_Q^2$ and taken outside of the k_0^2 integral [22]. In this way one arrives at the familiar convolution form

$$f_{q/P}(x) = \sum_{Q=U,D} \int_0^1 dy \int_0^1 dz \delta(x - yz) f_{q/Q}(z) f_{Q/P}(y) \quad (3.19)$$

and a similar expression with $q \rightarrow \bar{q}$, where the parent quark distribution in the proton $f_{Q/P}$ is given by eq.(3.6), and $f_{q/Q}$ ($f_{\bar{q}/Q}$) is the quark (antiquark) distribution within an on-shell parent quark which is obtained by evaluating the Feynman diagrams shown in fig.3.

The quark and antiquark distributions in the parent quark obtained from the diagrams of fig.3 can be expressed as

$$f_{u/U}(x) = Z_Q \delta(x - 1) + \frac{1}{3} F_{q/Q}(x) + \frac{5}{6} F_{q(\pi)/Q}(x) \quad (3.20)$$

$$f_{d/U}(x) = \frac{2}{3} F_{q/Q}(x) + \frac{1}{6} F_{q(\pi)/Q}(x) \quad (3.21)$$

$$f_{\bar{u}/U}(x) = \frac{1}{6} F_{q(\pi)/Q}(x) \quad (3.22)$$

$$f_{\bar{d}/U}(x) = \frac{5}{6} F_{q(\pi)/Q}(x). \quad (3.23)$$

The distributions for $Q = D$ are also determined from these expressions due to isospin symmetry. The detailed formulae for the distributions $F_{q/Q}(x)$ and

$$F_{q(\pi)/Q}(x) = \int_0^1 dy \int_0^1 dz \delta(x - yz) \int_{-\infty}^{\infty} dq_0^2 F_{q/\pi}(z, q_0^2) F_{\pi/Q}(y, q_0^2), \quad (3.24)$$

corresponding to the second and third diagrams of fig.3, respectively, can be obtained from the previous expressions (3.7)-(3.13) as follows: $F_{q/Q}(x)$, $F_{q/\pi}$ and $F_{\pi/Q}$ are given by expressions similar to eqs.(3.7), (3.10) and (3.11), respectively, but with the following replacements: (i) The nucleon spinor Γ_N is replaced by the quark spinor defined via the residue of the propagator $S(p)$: $\Gamma_Q(p) = Z_Q u_Q(p)$, where $u_Q(p)$ is a free Dirac spinor with mass M_Q normalized by $\bar{u}_Q(p) u_Q(p) = 2M_Q$. From eq.(3.18) it follows that this spinor satisfies the relation

$$\frac{1}{2p_-} \bar{\Gamma}_Q(p) \frac{\partial \Pi_Q(p)}{\partial p_+} \Gamma_Q(p) = 1 - Z_Q. \quad (3.25)$$

(ii) the polarizations $\Pi_N(x, p)$ and $\Pi_N(y, q_0^2; p)$ are replaced by $\Pi_Q(x, p)$ and $\Pi_Q(y, q_0^2; p)$. These are defined analogously to eqs. (3.8) and (3.13) by introducing the δ function insertions to fix the minus momentum components of the quark or the pion and the virtuality q_0^2 of the pion into Π_Q defined by eq. (3.16) instead of Π_N , and (iii) $F_{q/\pi}$ is given by the r.h.s. of eq. (3.10), but without the overall factor 2. We note that $f_{q/Q}$, and therefore also the distribution $f_{q/P}$ of eq. (3.19), involves an overall factor Z_Q , in accordance with our discussion following eq. (3.18).

From these expressions and the normalization (3.25), the validity of the number and momentum sum rules

$$\int_0^1 dx (f_{q/Q}(x) - f_{\bar{q}/Q}(x)) = \delta_{Q,q} \quad (3.26)$$

$$\int_0^1 dx \cdot x \left(f_{u/Q}(x) + f_{\bar{u}/Q}(x) + f_{d/Q}(x) + f_{\bar{d}/Q}(x) \right) = 1 \quad (3.27)$$

can be easily checked in the same way as outlined above for the parent quark distributions in the proton. (The number sum rule is a consequence of the Ward identity for the quark number current of the parent quark $\Lambda_{q/Q}^+(p, p) = \frac{\partial \Pi_Q(p)}{\partial p_+} \delta_{q,Q}$.) The validity of the number and momentum sum rules

$$\int_0^1 dx f_{q_v/P}(x) \equiv \int_0^1 dx \left(f_{q/P}(x) - f_{\bar{q}/P}(x) \right) = N_{q/P} \quad (3.28)$$

$$\int_0^1 dx \cdot x \left(f_{u/P}(x) + f_{\bar{u}/P}(x) + f_{d/P}(x) + f_{\bar{d}/P}(x) \right) = 1 \quad (3.29)$$

is then a consequence of eqs. (3.14), (3.15), (3.26), refbmom2 and (3.19).

Of particular interest is also the Gottfried sum

$$\begin{aligned} S_G &= \frac{1}{3} \int_0^1 dx \left(f_{u/P}(x) + f_{\bar{u}/P}(x) - f_{d/P}(x) - f_{\bar{d}/P}(x) \right) \\ &= \frac{1}{3} - \frac{4}{9} \int_0^1 dx F_{q/Q}(x) = \frac{1}{3} - \frac{4}{9} (1 - Z_Q), \end{aligned} \quad (3.30)$$

which shows that the deviation from the valence quark model result ($S_G = \frac{1}{3}$) is due to the decrease of the probability of the 'bare' valence quark state ($Z_Q < 1$) [28].

We now discuss our regularization scheme. Since the above expressions for the quark distributions involve loop integrals with one of the LC momentum components fixed, it is clear that we need a regularization scheme which can be formulated in terms of LC momenta. Two such schemes which have been discussed extensively in ref. [15] are the Lepage-Brodsky (LB) or invariant mass scheme [29], and the transverse cut-off (TR) scheme [30]. The basic graphs which are regularized in both schemes are the qq and $\bar{q}q$ bubble graphs $\Pi_s = \Pi_\pi$, the quark-diquark bubble graph Π_N and the quark self energy Π_Q ,

either for the case that all internal momentum components are integrated out or one of the LC momentum components is fixed. Concerning the LB scheme, it has been shown in detail for the case of Π_s in ref. [15] that, if all momentum components are integrated out, this scheme is equivalent to the covariant 3-momentum (or dispersion) cut-off scheme.⁹ Generally, if the intermediate state involves particles with masses m_1 and m_2 , the LB cut-off applied in the frame where the transverse components of the total momentum are zero ($\mathbf{p}_\perp = 0$) restricts the invariant mass of the state according to

$$\frac{\mathbf{k}_\perp^2 + m_1^2}{x} + \frac{\mathbf{k}_\perp^2 + m_2^2}{1-x} < \Lambda_{LB}^2, \quad (3.31)$$

where x and $1-x$ are the fractions of the total momentum component p_- carried by the two particles. The LB regulator Λ_{LB} is related to the 3-momentum cut-off Λ_3 by $\Lambda_{LB} = \left(\sqrt{m_1^2 + \Lambda_3^2} + \sqrt{m_2^2 + \Lambda_3^2} \right)$. For the case of $\Pi_s = \Pi_\pi$ we have $m_1 = m_2 = M_Q$, and the value of Λ_3 is determined as usual by requiring that $f_\pi = 93MeV$. In the case of the graphs Π_N (Π_Q) we have $m_1 = M_Q$, while m_2 is the mass parameter in the dispersion representation of τ_s (τ_π). In order not to increase the number of parameters, we will take the same value of Λ_3 for all graphs $\Pi_s = \Pi_\pi$, Π_N and Π_Q .

Concerning the TR cut-off scheme, it has been discussed in ref. [15] that the use of this scheme requires a mass renormalization procedure, since the basic self energies Π_α ($\alpha = s, \pi, N, Q$) involve also logarithmically divergent longitudinal momentum (k_-) integrals, which are not affected by the TR

⁹By 'covariant 3-momentum cut-off scheme' we mean the procedure where the 3-momentum cut-off is introduced in the particular Lorentz frame where the total momentum of the two-body (qq , $\bar{q}q$, or quark-diquark) state is zero ($\mathbf{p} = 0$), and the result is 'boosted' to a general frame. For the graphs Π_α ($\alpha = s, \pi, N, Q$) considered here, this 'boosting' simply means the replacement $p_0^2 \rightarrow p^2$, and for Π_N and Π_Q also $p_0\gamma^0 \rightarrow \not{p}$. It is known that this procedure is equivalent to the dispersion cut-off scheme [31].

regularization prescription $|\mathbf{k}_\perp| < \Lambda_{TR}$. In this scheme one has therefore to impose the pion, the diquark and the nucleon masses as renormalization conditions rather than to relate them to the parameters g_π , g_s and r_s via the pole conditions. For example, if we impose the condition $1 + 2g_s\Pi_s(M_D^2) = 0$ for some fixed M_D , the t-matrix τ_s in eq. (2.3) can be re-written in the renormalized form $\tau_s = 2i/(\Pi_s(k^2) - \Pi_s(M_D^2))$, which is formally independent of g_s and free of divergencies due to the longitudinal momentum integration. In the calculation using the TR cut-off we will impose the same value of M_D as obtained in the calculation using the LB cut-off.

4 Numerical results

In both the LB and TR regularization schemes we use $M_Q = 400MeV$ for the constituent quark mass, and determine the cut-off so as to reproduce $f_\pi = 93MeV$. This gives $\Lambda_3 = 593MeV$ for the equivalent 3-momentum cut-off in the LB scheme, and $\Lambda_{TR} = 407MeV$ in the TR scheme. In the LB scheme, we then obtain $g_\pi = 6.92GeV^{-2}$ and $r_s = g_s/g_\pi = 0.727$ from the requirements $m_\pi = 140MeV$ and $M_N = 940MeV$, respectively, and the resulting scalar diquark mass becomes $M_D = 600MeV$.¹⁰ As we explained earlier, in the TR scheme we use the same value $M_D = 600MeV$, and rewrite the t-matrices τ_π and τ_s , which are needed to calculate the distribution functions, in terms of m_π and M_D such that they become independent of g_π and r_s .

Our results for the valence and sea quark distributions are shown in figs. 4-7 both for the LB and the TR cut-off scheme. As we have explained in sect.1, in order to make contact to the empirical distributions extracted

¹⁰The current quark mass obtained from the gap equation is $m = 5.96MeV$ in the LB scheme.

from the measured structure functions, we have to evolve our calculated distributions from the low energy scale $\mu^2 = Q_0^2$ to the value $\mu^2 = Q^2$ where empirical parametrizations are available. For this Q^2 evolution we use the computer code of ref. [32] to solve the DGLAP equation in the next-to-leading order. (For the Q^2 evolution we use $N_f = 3$, $\Lambda_{QCD} = 250 MeV$.) We will compare our evolved distributions to the parametrizations of ref.[33] for $Q^2 = 4 GeV^2$. Both the calculated and the empirical distribution functions refer to the \overline{MS} renormalization and factorization scheme. The value of Q_0^2 is treated as a free parameter which is determined so as to reproduce the overall features of the empirical valence quark distributions at $Q^2 = 4 GeV^2$. In this way we obtain a value of $Q_0^2 = 0.16 GeV^2$, i.e; Q_0 is equal to our constituent quark mass M_Q .

Let us first discuss the valence quark distributions shown in figs. 4 and 5. Although we do not show the results of the pure valence quark model (no pions), we note that the input distributions at $\mu^2 = Q_0^2$ shown here are softer than in the case without pionic cloud effects, that is, the pionic effects reduce the peak heights of the valence quark distributions and increase their support at low x . The integral over the input distributions shows that at $\mu^2 = Q_0^2$ the valence quarks carry 92 % (87 %) of the nucleon's LC momentum for the case of the LB (TR) cut-off. The rest is carried by the sea quarks. This reduction of the peak heights due to pionic effects has a beneficial effect on the overall behaviour of the valence quark distributions, although it is insufficient in particular for the d quark in the LB scheme. The input distributions are still rather stiff even when pionic effects are taken into account, which necessitates the use of a low value of Q_0^2 in order to approach the empirical distributions via the Q^2 evolution. We can expect some improvement concerning this point

in a full Faddeev calculation, since in the present static approximation the size of the nucleon is too small, corresponding to momentum distributions which are too stiff.

In the LB cut-off scheme, the input distributions are zero for large (and also very small) values of x , and therefore the output distributions (at $Q^2 = 4\text{GeV}^2$) show a too strong variation with x compared to the empirical ones. On the contrary, for the TR cut-off the input distributions are non-zero in the whole region of x , which leads to a smoother behaviour of the output distributions.¹¹ This is the same feature as noted in ref. [15] for the quark distribution in the pion, and indicates that for phenomenological applications the TR cut-off seems to be superior over the LB cut-off. On the other hand, as we have explained earlier, the shortcoming of the TR cut-off scheme is that the diquark mass must be treated as a free parameter since in this scheme mass renormalizations are necessary in order to get finite results.

In our calculation, the difference between the valence u and d quark distributions reflects the scalar diquark correlations in the proton: Since the d quark appears inside the diquark and not as a spectator quark (see eq.(3.6)), its distribution is given by the convolution of two distributions (eq.(3.9)), which is more concentrated at low values of x compared to the spectator quark distribution. This is in agreement with the behaviour shown by the empirical distributions, and this observation was in fact one of the motivations to introduce diquark degrees of freedom also into the bag model description of the nucleon structure functions [3].

¹¹For the TR cut-off, the input distributions show a sharp increase when x becomes very close to 1. Since the computer code used for the Q^2 evolution [32] requires an input distribution which vanishes for $x = 1$, we artificially modified it for x very close to 1 such that it goes like $(1 - x)^n$ with some power n . ($n = 10$ was used in the actual calculation.)

We now turn to the antiquark distributions shown in figs. 6 and 7. As in the case of the valence quark distributions, the TR cut-off scheme leads to an overall better agreement with the empirical distributions than the LB scheme. The enhancement of \bar{d} over \bar{u} is clearly seen both in the input and the output distributions. Since the numerical value of the probability of the quark state without pion cloud is $Z_Q = 0.84$ ($Z_Q = 0.83$) for the LB (TR) cut-off scheme, the Gottfried sum (3.30) becomes $S_G = 0.262$ ($S_G = 0.257$), compared to the experimental value ¹² reported by the NM collaboration [1] $S_G = 0.235 \pm 0.026$. Our results for the difference $f_{\bar{d}/P} - f_{\bar{u}/P}$ are shown in fig. 8. We see that with our value of Q_0^2 which has been chosen such as to reproduce the overall behaviour of the valence quark distributions, the calculated difference is smaller than the empirical one for intermediate values of x , but larger for small x . Concerning the ratio \bar{u}/\bar{d} , there are also data from Drell- Yan processes [35] which give $\bar{u}/\bar{d} = 0.51 \pm 0.04 \pm 0.05$ at $x = 0.18$, compared to our calculated value of 0.68 (0.70) at $Q^2 = 4\text{GeV}^2$ for the LB (TR) cut-off. This, too, shows that the observed flavor asymmetry of the Dirac sea is larger than our calculated one in this range of x .

5 Summary and outlook

In this paper we used the framework of the relativistic Faddeev equation in the NJL model to calculate the quark LC momentum distributions in the nucleon. As a first step towards a full Faddeev calculation, we used the nucleon vertex functions obtained in the simple static approximation to the Faddeev kernel, and included pionic cloud effect approximately using the

¹²It has been shown that the Gottfried sum is almost unchanged by the Q^2 evolution [5, 34].

familiar convolution formalism. We can summarize our results as follows: First, we have shown a method based on a straight forward Feynman diagram evaluation, which we believe to be best suited for the calculation of the distribution functions in the Faddeev framework. Besides being simple and straight forward, the method also guarantees the validity of the number and momentum sum rules from the outset. Second, we discussed two regularization schemes which can be formulated in terms of LC coordinates, and which preserve the number and momentum sum rules. Based on our numerical results we concluded that for the description of the momentum distributions in the nucleon the transverse momentum cut-off scheme is superior over the invariant mass regularization scheme, which is similar to the situation found previously for the momentum distribution in the pion. Third, we have shown that the resulting distribution functions reproduce the overall behaviours of the empirical ones if the low energy scale for the Q^2 evolution is taken to be about the same as the constituent quark mass (400MeV in our calculation). Such a low value is required since the input valence quark distributions calculated in our model are rather stiff, although the pionic cloud effects served to soften them compared to the pure valence quark results. In this respect, a full Faddeev calculation which gives larger and more realistic nucleon radii, as well as the inclusion of higher mass diquark channels (axial vector diquark channel) are expected to improve the situation. We have also shown that the value for the Gottfried sum obtained in this simple calculation is in basic agreement with the experimental one.

The formulation and results of this work can be used as a basis for at least the following three extensions: First, one could easily use the present framework to calculate the quark spin distributions, provided that the axial

vector diquark ($J = 1$) channel is also taken into account. Second, one should use the full Faddeev vertex functions to calculate the quark momentum distributions. As we have noted in sect.1, the most convenient way for this purpose might be first to go to the moment space and then to reconstruct the distribution functions. The third extension concerns the case of finite density: For a finite density calculation the full Faddeev framework seems to be intractable, and approximations like the static approximation used in this paper might be unavoidable. For this purpose, however, it is necessary first to construct an equation of state for nuclear matter based on the Faddeev (quark-diquark) picture of the single nucleon, similar to the Guichon equation of state [36] which is based on the MIT bag picture of the single nucleon. The construction of such an equation of state and its applications are now under consideration [37].

ACKNOWLEDGEMENTS

The authors would like to thank M. Miyama and S. Kumano for the computer program used for the Q^2 evolution (ref. [32]). One of the authors (W.B.) is grateful to A. W. Thomas, A. W. Schreiber, K. Suzuki and K. Tanaka for discussions on the nucleon structure function.

References

- [1] SLAC-MIT collaboration, G. Miller et al., Phys. Rev. **D 5** (1972) 528;
BCDMS collaboration, A.C. Benvenuti et al., Phys. Lett. **B 223** (1989) 485;
NM collaboration, M. Arneodo et al., Phys. Rev. **D 50** (1994) R1;
H1 collaboration, C. Adloff et al., Z. Phys. **C 74** (1997) 191
ZEUS collaboration, J. Breitweg et al., Z. Phys. **C 74** (1997) 207.
- [2] R.K. Ellis, W.J. Stirling and B.R. Webber, QCD and Collider Physics, Cambridge Univ. Press, 1996, chap.4.
- [3] F.E. Close and A.W. Thomas, Phys. Lett. **B 312** (1988) 227
A.W. Schreiber, A.I. Signal and A.W. Thomas, Phys. Rev. **D 44** (1991) 2653.
- [4] F.M. Steffens and A. W. Thomas, Phys. Rev. **C 55** (1997) 900.
- [5] S. Kumano, Phys. Rep. **303** (1998) 183.
- [6] J.C. Collins, D. Soper and G. Sterman, Perturbative Chromodynamics, ed. A.H. Mueller, World Scientific, Singapore, 1989, p.1.
- [7] V.N. Gribov and L.N. Lipatov, Sov. J. Nucl. Phys. **15** (1972) 438 and 675;
G. Altarelli and G. Parisi, Nucl. Phys. **B 126** (1977) 298;
Yu.L. Dokshitzer, Sov. Phys. JETP **46** (1977) 641.
- [8] Y. Nambu and G. Jona-Lasinio, Phys. Rev. **122** (1960) 345; **124** (1961) 246.

- [9] R. Brockmann, W. Weise and E. Werner, Phys. Lett. **B 122** (1983) 201;
D. Ebert and H. Reinhardt, Nucl. Phys. **B 271** (1986) 188;
U. Vogl and W. Weise, Prog. Part. Nucl. Phys. **27** (1991) 195;
M. Kato, W. Bentz, K. Yazaki and K. Tanaka, Nucl. Phys. **A 551** (1993)
541.
- [10] N. Ishii, W. Bentz and K. Yazaki, **B 318** (1993) 26;
N. Ishii, W. Bentz and K. Yazaki, Nucl. Phys. **A 578** (1995) 617.
- [11] U. Zückert, R. Alkofer, H. Weigel and H. Reinhardt, Phys. Rev. **55**
(1997) 2030;
S. Huang and J. Tjon, Phys. Rev. **C 49** (1994) 1702;
C. Hanhart and S. Krewald, Phys. Lett. **B 344** (1995) 55.
- [12] H. Asami, N. Ishii, W. Bentz and K. Yazaki, Phys. Rev. **C 52** (1996)
3388.
- [13] H. Weigel, L. Gamberg and H. Reinhardt, Mod. Phys. Lett. **A 11** (1996)
3021;
M. Wakamatsu and T. Kubota, Chiral symmetry and the nucleon spin
structure functions, hep-ph/9809443.
- [14] K. Kusaka, G. Piller, A.W. Thomas and A.G. Williams, Phys. Rev. **D**
55 (1997) 5299.
- [15] W. Bentz, T. Hama, T. Matsuki and K. Yazaki, NJL model on the light
cone and pion structure function, Nucl. Phys. **A**, in press.
- [16] H. Mineo, H. Asami, W. Bentz and K. Yazaki, work in progress.

- [17] A. Buck, R. Alkofer and H. Reinhardt, Phys. Lett. **B 286** (1992) 29.
- [18] N. Ishii, W. Bentz and K. Yazaki, Phys. Lett. **B 301** (1993) 165.
- [19] G. Hellstern and C. Weiss, Phys. Lett. **B 351** (1995) 64.
- [20] K. Suzuki, T. Shigetani and H. Toki, Nucl. Phys. **A 573** (1994) 541;
R. Jakob, P.J. Mulders and J. Rodrigues, Nucl. Phys. **A 626** (1997) 937.
- [21] R.T. Cahill, C.D. Roberts and J. Praschifka, Aust. J. Phys. **42** (1989) 129;
R.T. Cahill, Nucl. Phys. **A 543** (1992) 630.
- [22] R.L. Jaffe, 1985 Los Alamos School on Relativistic Dynamics and Quark Nuclear Physics, eds. M.B. Johnson and A. Pickleseimer, Wiley, New York, 1985.
- [23] R.L. Jaffe, Nucl. Phys. **B 229** (1983) 205.
- [24] S.A. Kulagin, G. Piller and W. Weise, Phys. Rev. **C 50** (1994) 1154.
- [25] A. Szczurek, A. Buchmann and A. Faessler, J. Phys. **G 22** (1996) 1741;
J. Speth and A.W. Thomas, Adv. Nucl. Phys. **24** (1997) 83;
K. Suzuki and W. Weise, Nucl. Phys. **A 634** (1998) 141.
- [26] F. Zamani, Phys. Rev. **C 58** (1998) 3641.
- [27] S.A. Kulagin, W. Melnitchouk, T. Weigl and W. Weise, Nucl. Phys. **A 597** (1996) 151.

- [28] A.W. Schreiber, P.J. Mulders and A.I. Signal, Phys. Rev. **D 45** (1992) 3069.
- [29] G.P. Lepage and S.J. Brodsky, Phys. Rev. **D 22** (1980) 2157.
- [30] F. Lenz, K. Ohta, M. Thies and K. Yazaki, to be published.
- [31] T. Hatsuda and T. Kunihiro, Phys. Rep. **247** (1994) 221.
- [32] M. Miyama and S. Kumano, Comp. Phys. Commun. **94** (1996) 185.
- [33] A.D. Martin, W.J. Stirling and R.G. Roberts, Phys. Rev. **D 50** (1994) 6734.
- [34] D.A. Ross and C.T. Sachrajda, Nucl. Phys. **B 149** (1997) 497.
- [35] A. Baldit et al., Phys. Lett. **B 332** (1994) 244.
- [36] P.A.M. Guichon, Phys. Lett. **B 200** (1988) 235.
- [37] W. Bentz, A.W. Thomas and K. Yazaki, work in progress.

Figure captions

1. Graphical representation of the quark LC momentum distribution in the Faddeev framework. The single (double) line denotes the quark propagator (scalar diquark t-matrix), the hatched circle stands for the quark- diquark vertex function, and the operator insertion denoted by a cross stands for $\gamma^+ \delta(k_- - p_- x)(1 \pm \tau_z)/2$ for the $U(D)$ quark distribution. The second diagram stands symbolically for those 2 diagrams obtained by inserting the cross into both particle lines in the diquark. The quark-diquark vertex contains the isospin operator τ_2 . The diagram where the operator insertion is made on the exchanged quark is not shown here since it does not contribute in the static approximation.
2. Feynman diagrams which have to be evaluated in addition to those shown in fig.1 due to the presence of the pion cloud. Here the dashed line indicates the $\bar{q}q$ t-matrix in the pionic channel, and the other lines are as in fig.1. The second diagram stands symbolically for those 2 diagrams obtained by inserting the cross into both the q and \bar{q} lines in the pion. The dots indicate all remaining diagrams where the pion line is attached to a quark in the diquark.
3. Graphical representation of the quark distribution within an on-shell parent quark. The meaning of the lines is as in figs.1 and 2. The quark spinor $\Gamma_Q(p)$ is associated with the incoming and outgoing quark lines in all diagrams. The operator insertion in the first diagram stands for $\gamma^+ \delta(p_- - p_- x)(1 \pm \tau_z)/2$, and in the other diagrams for $\gamma^+ \delta(k_- - p_- x)(1 \pm \tau_z)/2$ for the u(d) quark distributions. The third diagram

stands symbolically for those 2 diagrams obtained by inserting the cross into both the q and \bar{q} lines in the pion.

4. LC momentum distributions of the valence u -quark in the proton, using the LB (solid lines) and TR (dashed lines) regularization scheme. The lines associated with $Q_0^2 = 0.16\text{GeV}^2$ show the NJL model results, and the lines associated with $Q_0^2 = 0.16\text{GeV}^2$ show the results obtained by the QCD evolution in next-to-leading order from $Q_0^2 = 0.16\text{GeV}^2$ to $Q^2 = 4\text{GeV}^2$, using $\Lambda_{QCD} = 0.25\text{GeV}$ and $N_f = 3$. The dotted line shows the parametrization for $Q^2 = 4\text{GeV}^2$ obtained in ref. [33] by analyzing the experimental data.
5. LC momentum distributions of the valence d -quark in the proton. For explanation of the lines, see the caption to fig. 4.
6. LC momentum distributions of the \bar{u} -quark in the proton. For explanation of the lines, see the caption to fig. 4.
7. LC momentum distributions of the \bar{d} -quark in the proton. For explanation of the lines, see the caption to fig. 4.
8. The difference of \bar{d} and \bar{u} -quark momentum distributions in the proton. For explanation of the lines, see the caption to fig. 4.

Figure 1

$$f_{Q/P}(\mathbf{x}) = \frac{1}{2} \left[\text{Diagram 1} + \text{Diagram 2} \right]$$

The figure shows two Feynman diagrams enclosed in large square brackets, separated by a plus sign. The first diagram on the left consists of two gray circular vertices. The left vertex has three external lines labeled 'p' entering from the left. The right vertex has three external lines labeled 'p' exiting to the right. Two arcs connect the vertices: an upper arc with momentum 'k' and a lower arc with momentum 'p-k'. A cross symbol is placed on the upper arc. The second diagram on the right also has two gray circular vertices with three external lines labeled 'p' on each. Two arcs connect the vertices: an upper arc with momentum 'p-q' and a lower arc with momentum 'q'. A self-energy loop is attached to the lower arc, with momentum 'q' entering from the vertex and momentum 'q-k' exiting back to the vertex. A cross symbol is placed on the upper part of this loop.

Figure 2

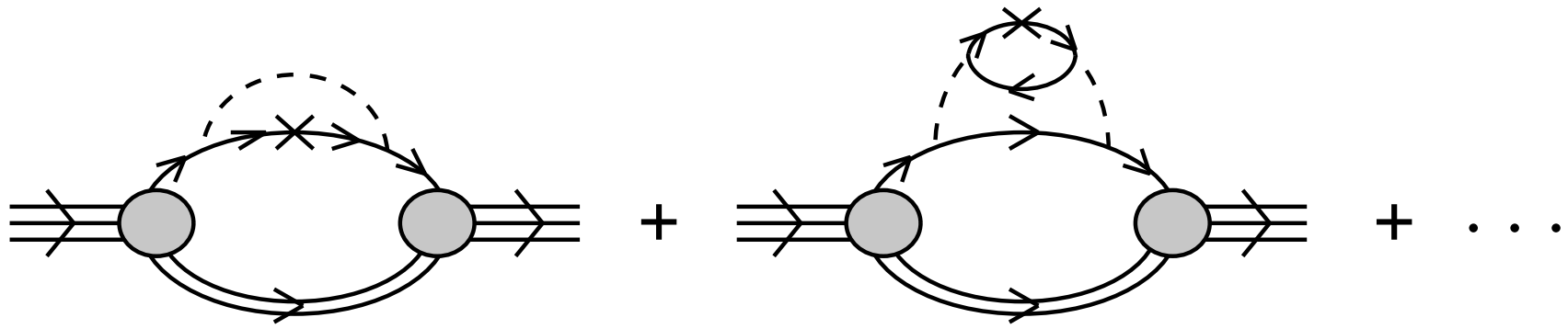


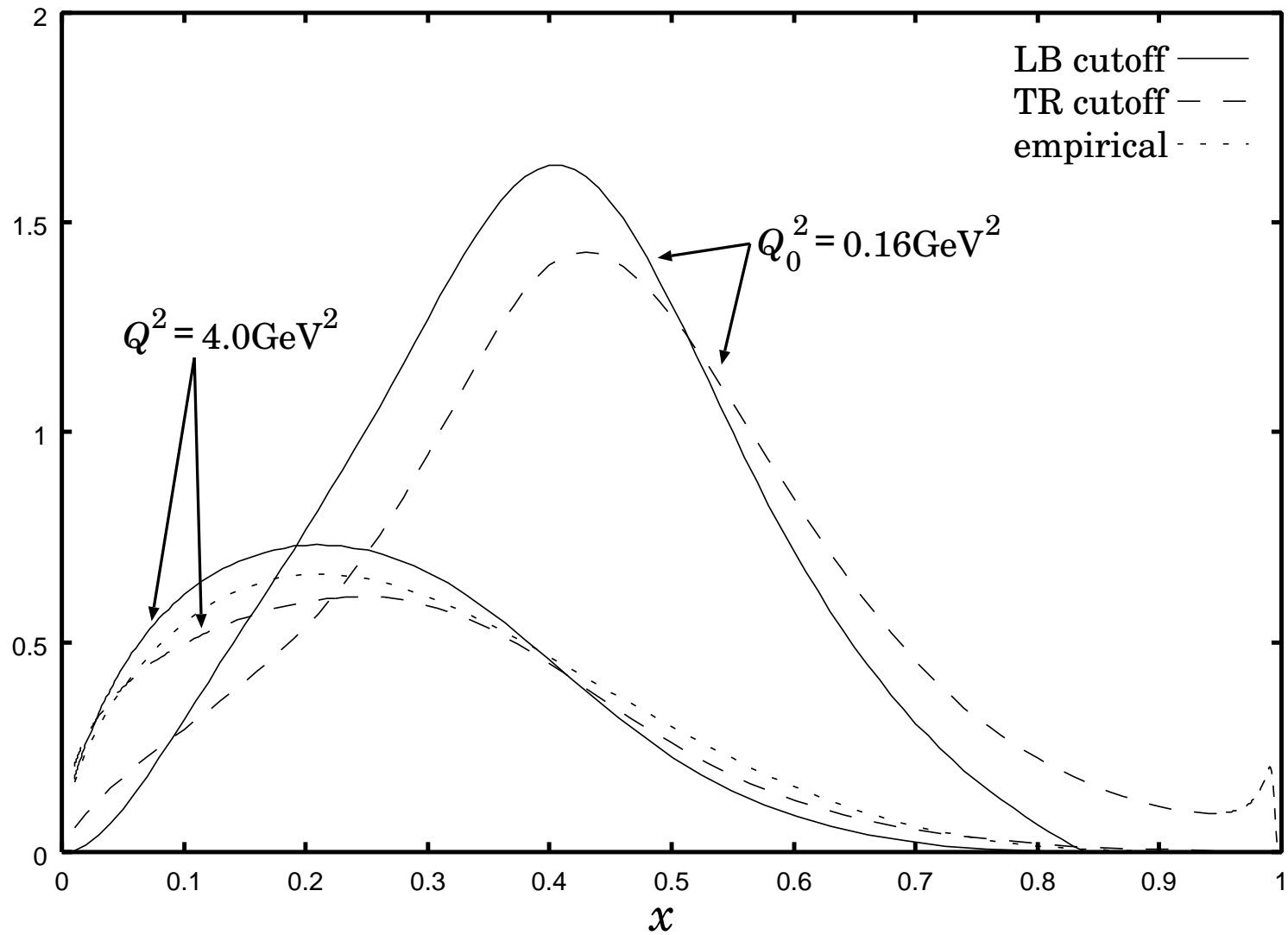
Figure 3

$$f_{q/Q}(\mathbf{x}) = \frac{1}{2} \left[\begin{array}{c} \text{Diagram 1} + \text{Diagram 2} \\ \text{Diagram 3} \end{array} \right]$$

The figure shows three Feynman diagrams representing terms in a sum. The first two diagrams are enclosed in a large square bracket, and the third is added below it.

- Diagram 1:** A horizontal line with two vertices marked with an 'x'. The left vertex is labeled 'p' and the right vertex is labeled 'p'. Arrows on the line point from left to right.
- Diagram 2:** A horizontal line with three vertices marked with an 'x'. The left and right vertices are labeled 'p', and the middle vertex is labeled 'k'. Arrows on the line point from left to right. A dashed arc connects the left and right vertices, labeled 'p-k' above it.
- Diagram 3:** A horizontal line with three vertices marked with an 'x'. The left and right vertices are labeled 'p', and the middle vertex is labeled 'p-q'. Arrows on the line point from left to right. A dashed arc connects the left and right vertices, labeled 'q' above it. Inside this arc is a circular loop with two vertices marked with an 'x'. The top vertex is labeled 'k' and the bottom vertex is labeled 'k-q'. Arrows on the loop indicate a clockwise direction.

$xf_{u_v}/P(x)$



$xf_{d_v/P}(x)$

